The effectiveness of an active noise control system with remote microphones technique in a tractor cabin[1]

Francesco Mori[a]* | Andrea Santoni[a] | Patrizio Fausti[a] | Francesco Pompoli[a] | Pietro Nataletti[b] | Paolo Bonfiglio[c]

[a] Dipartimento di Ingegneria, Università degli studi di Ferrara, Via Saragat, 1, 44122 Ferrara
[b] Istituto Nazionale per l'Assicurazione contro gli Infortuni sul Lavoro, Via di Fontana Candida, 1, 00078 Roma
[c] Materiacustica Srl, Via C. Ravera, 15/A, 44122 Ferrara
* Corresponding author: francesco.mori@unife.it

Ricevuto: 19/1/2025
Accettato: 5/3/2025

DOI: 10.3280/ria1-2025oa19189
ISSNe: 2385-2615

This paper presents a preliminary study of an active noise control (ANC) system implemented on a tractor cabin. This system employs a multi-channel feedforward configuration, with two error microphones and two control loudspeakers positioned in the cabin and an external reference microphone. Furthermore, the system implements the remote microphone technique (RMT), which allows to place the error microphones at a given distance from the region where the quiet zone is to be created, in this case around a head used for binaural measurements. To evaluate the effectiveness of the ANC system, simulated narrowband and broadband disturbance signals are generated through an acoustic source external to the cabin. Despite a reduction in the performance compared to the case without the RMT, caused by internal modelling of the signals, the developed system demonstrates its potentiality for a real application, where the error microphones cannot be left close to the region where noise has to be cancelled.
Keywords: active noise control, tractor, remote microphones technique, multi-channel feedforward, acoustic control, confined space

L'efficacia di un sistema di controllo attivo del rumore con tecnica dei microfoni remoti nella cabina di un trattore
Questo articolo mostra uno studio preliminare di un sistema di controllo attivo del rumore (ANC) implementato sulla cabina di un trattore. Tale sistema sfrutta una configurazione feedforward multi-canale, con due microfoni di errore e due altoparlanti di controllo posizionati in cabina e un microfono di riferimento esterno. Inoltre, il sistema impiega la tecnica dei microfoni remoti (RMT), che consente di posizionare i microfoni di errore a una data distanza dalla zona in cui si vuole creare la zona di quiete, in questo caso attorno alla testa di un manichino utilizzato per misure binaurali. Per la valutazione dell'efficacia del sistema ANC vengono generati segnali di disturbo simulati, a banda stretta e a banda larga, attraverso una sorgente acustica posizionata esternamente alla cabina. I risultati mostrano che, nonostante una riduzione delle prestazioni rispetto al caso senza RMT causata dalla modellazione interna dei segnali, il sistema sviluppato dimostra una potenzialità per un'applicazione reale, dove i microfoni di errore non possono essere lasciati in prossimità della zona in cui si vuole cancellare il rumore.
Parole chiave: controllo attivo del rumore, trattore, tecnica dei microfoni remoti, feedforward multi-canale, controllo acustico, campo confinato

1 | Introduction

Drivers in a tractor cabin are typically exposed to loud noise for prolonged time [1-4]. The noise perceived inside the cabin is typically dominated by low-frequency harmonics [5], mainly in the range between 20 Hz and 1000 Hz, coming from the most relevant noise sources, such as the engine, the exhaust and the cooling fan [6-8]. The attenuation of this low-frequency noise with traditional passive solutions is difficult to be realized [9-11], due to the limited space inside the cabin and the necessity to guarantee visibility to the driver in all the directions through the windowed walls. Furthermore, the acoustic characteristics of the glass walls create additional challenges for noise control, as they generate multiple reflections that contribute to a complex sound field inside the cabin. The use of hearing protection devices allows for a noise control localized at the driver's ears [12]. However, the prolonged use of these devices represents a constraint causing discomfort for many people. Furthermore, hearing protection devices typically show a limited performance in the frequency range below 500 Hz.

In this framework, an active noise control (ANC) system can represent a valid alternative solution to attenuate the noise in the low-frequency range [13,14]. In the broadest sense of the term, an ANC system is an electroacoustic device which computes through an algorithm and generates, by means of a control loudspeaker, an "anti-noise" signal with equal amplitude and opposite phase with respect to an undesired noise [15,16]. The superposition of these two signals makes them delete

[1] Vincitore del premio "Gino G. Sacerdote" edizione 2025.

each other in a region of space denominated "zone of quiet". The zone of quiet is typically created around the position of a microphone, called "error microphone", which senses the residual noise to be processed and minimized through the algorithm. However, the positioning of the error microphone in the spatial region where the noise must be attenuated is often hindered by physical constraints in real-world situations [17-19]. For instance, on industrial or agricultural vehicles, where the target is the attenuation of the noise perceived by the driver, it is necessary to create a zone of quiet around the head, maintaining the error microphone at a certain distance. To overcome this issue, different techniques, denominated "virtual sensing techniques", were proposed in the literature, permitting to create a zone of quiet at a given distance from the error microphone [20]. These approaches aim at estimating the real-time acoustic field at the target zone based on the data collected from the error microphone placed at a certain distance.

Two types of techniques exist. The first class of algorithms requires a preliminary modelling of the physical system to process the data sensed from the error microphone in the real-time application [21-24]. The performance of the ANC exploiting this class of algorithms depends heavily on the accuracy of the system model, obtained during the preliminary identification and it is sensitive to the location of the physical error microphones. The second class does not need a preliminary identification of the impulse responses of the physical system, but estimates the acoustic field through the sensed data [25], fitting polynomials [26], applying Kalman's filtering or making some simplified hypothesis for the estimation [27,28]. As can be imagined, even though this class of techniques can be more flexible and can be extended to cases with the need of tracking capability [29-32], these methods require a higher computational demand or introduce some limitations in the applications to reduce the computational cost.

This paper is aimed at investigating the applicability of an ANC system with the Remote Microphone Technique (RMT) inside the cabin of a tractor. This method belongs to the first category of techniques, since it estimates the acoustic field at the virtual location by filtering the data sensed by the error microphone through a preliminary modelled transfer function. This ANC system is developed in a multi-channel feedforward configuration, with two error microphones, two control loudspeakers and one reference microphone. The zone of quiet is created at the ears of a head & torso simulator used for binaural measurements. The tests for the validation of the system were carried out on a tractor cabin in a hemi-anechoic chamber, with a simulated disturbing noise source placed outside the cabin, generating both narrowband and broadband signals. Section 2 illustrates in detail the developed algorithm with the RMT. Section 3 describes the experimental setup used for the tests, distinguishing the devices involved during the preliminary stage and those ones employed in the final application. Section 4 discusses the results obtained with the implemented ANC system, comparing the cases with the noise directly cancelled at the ears and with the RMT. Furthermore, the extension of the zone of quiet and the acoustic field in the proximity of the head is analysed. Finally, Section 5 reports the conclusions of this study and discusses the possible future developments of this work.

2 | The ANC algorithm with RMT

The Remote Microphone Technique (RMT) belongs to the first class of methods, requiring a preliminary identification of the physical system. With reference to Fig. 1, the algorithm with the RMT can be structured in three stages: two trainings and the real-time operations. Positions $P_i (i = 1, 2)$ indicate the locations where the error microphones are physically placed during both the training stages and real-time operations, sensing the error signals $e_{p,i}(n)$. Positions $V_l (l = 1, 2)$ indicate the locations where the error microphones are physically placed only during the training stages, defining the position of the zone of quiet. During the real-time operations, the sensors in these positions are removed and the virtual error signals $e_{v,i}(n)$ are estimated starting from the physical error signals $e_{p,i}(n)$.

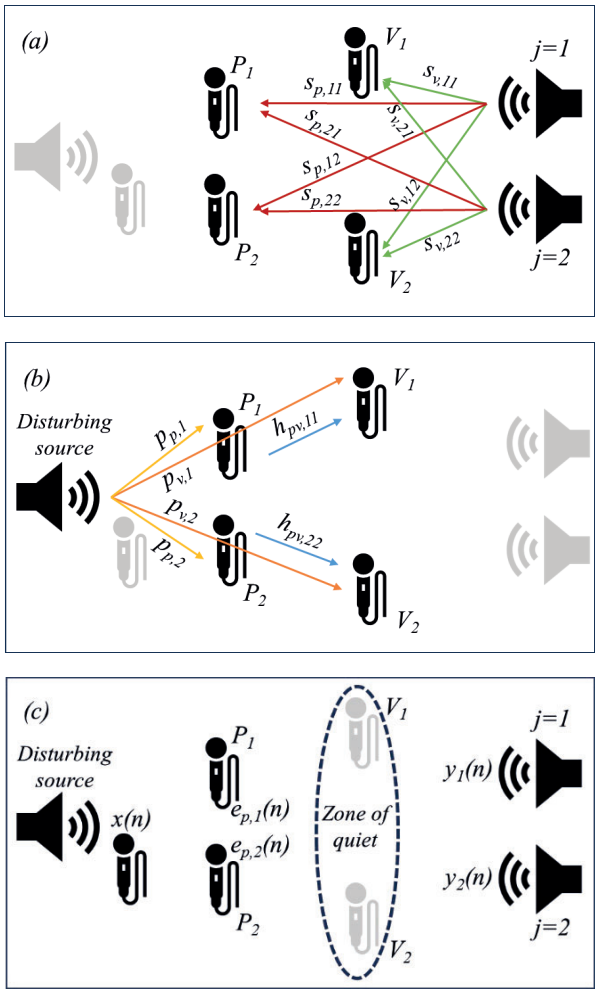

Fig. 1 – Stages of the RMT: (a) secondary paths identification, (b) identification of the physical-virtual impulse responses and (c) final system. The devices not involved in the stage are depicted in grey

Fasi della RMT: (a) identificazione dei percorsi secondari, (b) identificazione delle risposte all'impulso fisico-virtuali e (c) sistema finale. I dispositivi non coinvolti nella fase sono indicati in grigio

Furthermore, during the real-time operations, the $j = th$ control source ($j = 1, 2$) generates the anti-noise signal $y_j(n)$, while the reference microphone measures the reference signal $x(n)$.

In the first stage (Fig. 1(a)), the physical and the virtual secondary paths are estimated. The physical secondary paths $s_{p,jl}$ (indicated with red arrows) are defined as the impulse responses between the $j = th$ control source and the $i = th$ error microphone in the physical position; the virtual secondary paths $s_{v,jl}$ (green arrows) as the impulse responses between the $j = th$ control source and the $l = th$ virtual error microphone. For the estimation of these paths several approaches can be used [16,33]. In this paper, the estimation is carried out through the generation of a white noise with the control loudspeaker and modelling a filter through a Least Mean Squares (LMS) approach, such that the difference between the filter output and the signal sensed by the microphone is minimized [15]. In the second stage (Fig. 1(b)), the impulse responses $h_{pv,il}$ (blue arrows) between the physical and the virtual positions are estimated. In the developed system, it is assumed that one physical error microphone is used for the estimation of the acoustic field only in the virtual position on the same side, thus considering $i = l$. The estimation of these impulse responses can be determined from the ratio between the spectra of the virtual primary path $p_{v,i}$ (orange arrows) and the physical primary path $p_{p,i}$ (yellow arrows). The virtual primary path is defined as the impulse response between the disturbing noise source and the virtual error microphone, while the physical primary path represents the impulse response between the disturbing noise source and the physical error microphone. These impulse responses are estimated with the same procedure employed for the secondary paths, but generating the white noise with the disturbing noise source. All these impulse responses are stored in the control unit as finite impulse response (FIR) filters and used for filtering the signals sensed with the error microphones in the physical positions during the real-time operations.

In the third stage (Fig. 1(c)), the microphones in the virtual positions can be removed, since the acoustic field at the virtual positions are estimated through the following real-time operations. An apex' is used to distinguish the estimated quantities from the real ones. The disturbance at the physical positions $d'_{p,i}(n)$ is estimated as:

$$d'_{p,i}(n) = e_{p,i}(n) - \sum_{j=1}^{2} s'_{p,ji} * y_j(n), \quad (1)$$

where * denotes a discrete convolutional product. With these data, the disturbance at the virtual locations can be computed as:

$$d'_{v,l}(n) = h'_{pv,il} * d'_{p,i}(n), \quad (2)$$

from which the error signals at the virtual positions are evaluated as:

$$e'_{v,l}(n) = d'_{v,l}(n) - \sum_{j=1}^{2} s'_{v,jl} * y_j(n). \quad (3)$$

These virtual signals can be employed as inputs for the ANC algorithm, for computing the adaptive filters necessary to drive the control sources and generate the zone of quiet at the virtual location. At this scope, any algorithm can be used in combination with the RMT. However, the Filtered-X Least Mean Squares (FXLMS) algorithm was chosen in this paper, for its simplicity of implementation, scalability and possibility of modifications. Considering the virtual error signals $e'_{v,l}(n)$ as inputs, this algorithm aims at minimizing the total energy estimated at the virtual error positions. Thus, defining M the length of the adaptive filters and N the length of the secondary paths, according to the theory of the FXLMS algorithm [34], the adaptive filters are updated as:

$$w_{j,m}(n+1) = w_{j,m}(n) - \mu \sum_{l=1}^{2} e'_{v,l}(n) x'_{jl}(n-m) \quad (4)$$

where $m = 0, 1, \ldots M - 1$, μ is the step-size parameter, determining the stability and regulating the convergence speed, and x'_{jl} represents the reference signal filtered with the virtual secondary paths:

$$x'_{jl}(n) = s'_{v,jl} * x(n). \quad (5)$$

The output signals $y_j(n)$ emitted by the control sources are computed as:

$$y_j(n) = w_j(n) * x(n). \quad (6)$$

The limit of this technique is the introduction of a causality constraint [35], since only the noise which is firstly sensed at the physical positions can be attenuated at the virtual positions. To overcome this issue, Shi et al. [36] introduced the use of independent virtual and physical paths rather than the related information between the virtual and physical locations to update the control filter, carrying out the computation in the frequency domain. However, the computational demand of this variation in the algorithm is huge.

3 | Experimental setup

Experimental tests were carried out on the cabin of a tractor Case IH Farmall 120U in a hemi-anechoic chamber (Fig. 2). The setup external to the cabin consists of an omnidirectional noise source, emitting both narrowband and broadband noise signals, placed in front of the cabin, about 65 cm far from the reference microphone. Inside the cabin (Fig. 3), the virtual error microphones (EVR and EVL) are allocated at the entrances to the ear canals of a head & torso simulator. They are used for the two training stages of the ANC system and for monitoring the noise cancellation when the ANC is turned on. Two physical error microphones (EPR and EPL), sensing the error signals when the ANC system is turned on, are placed in the anterior part of the cabin. In this scheme, the physical error microphone on the left side (EPL) is used to model the virtual error signal on the left side and the analogue happens for the right side. Two control loudspeakers, endowed with an amplifier, are positioned on a shelf behind the seat, at a height similar to the one of the head. Further-

more, an array of three monitoring microphones with a spacing of 5 cm is placed near the left ear of the manikin to monitor the extension of the zone of quiet.

The hardware driving the whole system is a National Instruments cRio-9063 real-time target with an embedded FPGA (Field Programmable Gate Array) for the deterministic processing of the signals, a 4-channels NI-9234 input module for the acquisition of the data and a 2-channels NI-9260 output module for the generation of the control signals. The real-time target generates and acquires the signals with a sampling frequency of 6.400 Hz, while the operations executed by the adaptive algorithm are scanned by a 40 MHz onboard clock. The tested algorithm was implemented on the hardware within the LabVIEW development environment, by compiling the code directly on the FPGA to have a processing system working in an autonomous way from the PC monitoring the experiments and driving the simulated noise source. During the code compilation, the operations contained in the algorithm are assigned to circuits able to work in parallel to optimize the processing time. All the arrays used to store signals and filters were implemented on blocks of memory (BRAM), instead of look-up tables (LUT RAM), which would have consumed the more limited resources that the FPGA uses for the logical operations. Moreover, a fixed-point data type was adopted to optimize the usage of resources, rather than floating-point data. The length of the adaptive filters, secondary paths and physical-virtual impulse responses is fixed to 1024 elements. A maximum output voltage of 1 V was imposed inside the implemented algorithm to avoid a large divergence of the control sources in the case of instability. Tests were carried out with both the classical FXLMS algorithm and the version with the RMT, to compare the performance of the two systems.

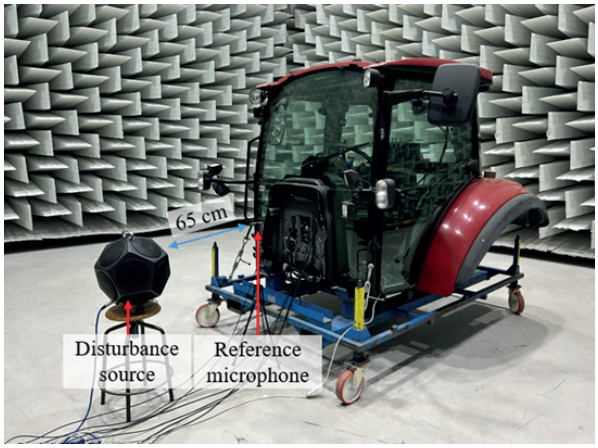

Fig. 2 – Setup sperimentale esterno alla cabina
Experimental setup outside the cabin

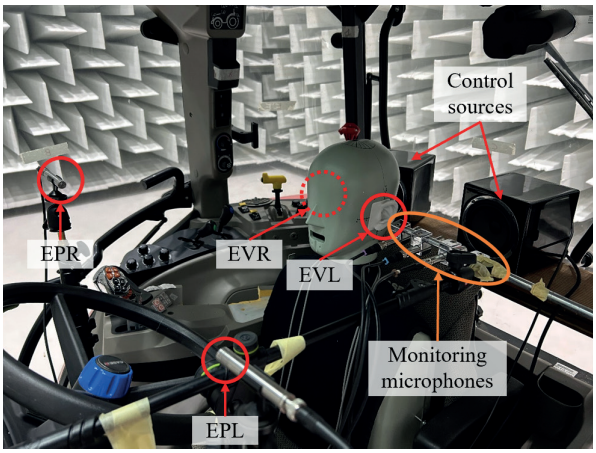

Fig. 3 – Setup sperimentale dentro la cabina (EV = microfoni virtuali, EP = microfoni fisici, L/R = sinistra e destra). L'array di microfoni di monitoraggio non è coinvolto nel sistema ANC
Experimental setup inside the cabin (EV = virtual microphones, EP = physical microphones, L/R = left and right). The array of monitoring microphones is not involved in the ANC system

4 | Results

4.1 | Transfer functions estimation

The secondary and the primary paths, used for the identification of the system impulse responses, are illustrated in Fig. 4 and Fig. 5 respectively, for both the physical and the virtual positions. These functions are shown in terms of transfer functions magnitude in the frequency domain for the sake of interpretation. The magnitude, expressed in dB, is defined as:

$$Magnitude = 20log_{10}(FFT\ Amplitude). \quad (7)$$

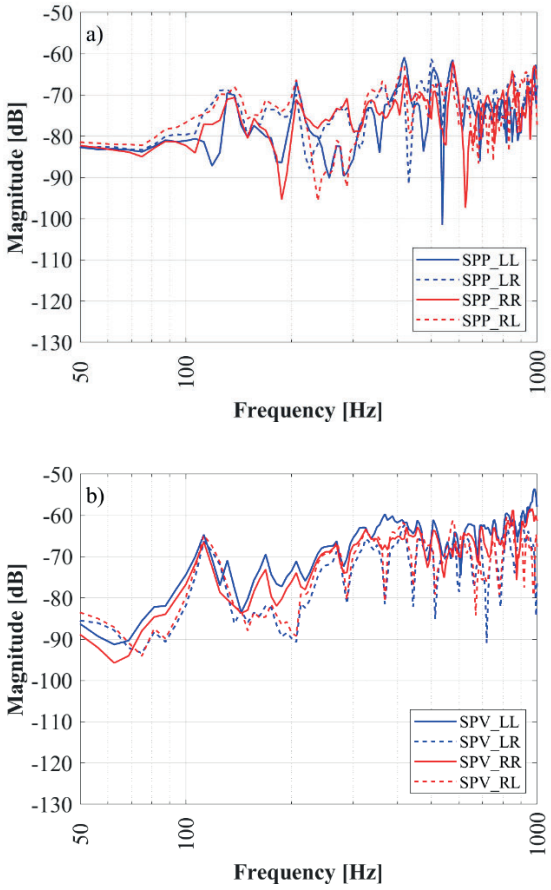

Fig. 4 – Percorsi secondari dei microfoni di errore (a) fisici (SPP) e (b) virtuali (SPV)
Secondary paths of (a) the physical (SPP) and (b) the virtual (SPV) error microphones

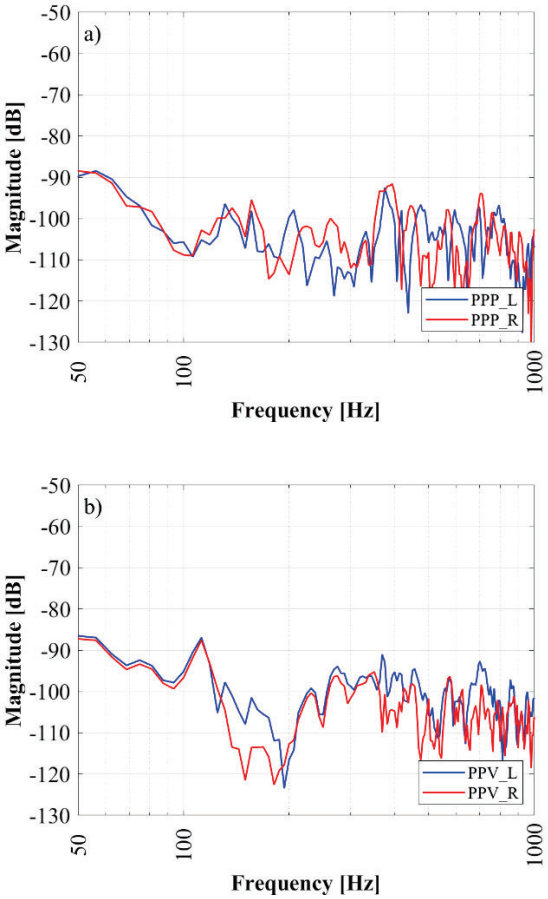

Fig. 5 – Percorsi primari dei microfoni di errore (a) fisici (PPP) e (b) virtuali (PPV)

Primary paths of (a) the physical (PPP) and (b) the virtual (PPV) error microphones

A negative value of the magnitude means that the filter output has a lower amplitude with respect to the filter input, while a positive value means the opposite. The estimation of these filters was carried out through the offline procedure based on the LMS algorithm described in [15], by injecting a white noise into the system (through the control sources for the secondary paths and the disturbing source for the primary paths) and sensing the signal with the error microphones. For this procedure, a filter length of 1024 elements and a step-size of 0.01 were considered. The estimation of the secondary paths is necessary for taking into consideration the latency provided by the control unit (mainly consisting in the analogue-to-digital and digital-to-analogue conversions and the anti-aliasing filter), the modal effects of the cavity and the characteristics of the control sources. On the other hand, the estimation of the primary paths is necessary for the successive computation of the physical-virtual impulse responses.

As can be observed, the secondary paths have an amplitude higher than the primary paths on the whole spectrum. If the disturbing noise source and the control sources were assumed to provide the same output, the previous condition must be considered necessary for avoiding the saturation of the control loudspeakers. However, considering that the amplitude of the disturbing noise source can differ from the one provided by the control loudspeakers, the previous condition becomes not sufficient and the saturation of the system becomes dependent also on the amplitude of the emitted disturbing signal and on the power limit of the control sources. Moreover, due to the multi-channel configuration, the effectiveness of the ANC system based only on these response functions is difficult to be evaluated, since it depends on the interaction between the four physical and the four virtual secondary paths. In addition, the amplitude of the cross secondary paths (from one control source to the error microphone on the opposite side) is comparable with the one of the direct paths (from one control source to the error microphone on the opposite side). Thus, all these contributions must be considered in the implementation of the algorithm.

The transfer functions employed in the RMT (HPV_L and HPV_R for the left and the right sides respectively), used to model the disturbance signals at the virtual positions starting from the sensing of the error signals at the physical positions, are reported in Fig. 6 for both the sides. These two functions were obtained as the ratio between the spectra of the virtual primary path on one side and the physical primary path on the same side. The positive values in these transfer functions mean that for some frequencies the sound pressure level at the virtual position assumes larger values with respect to the physical position. It can be evinced that the relative position of physical and virtual error microphones is not perfectly symmetric. However, the modelling of these two functions takes into consideration this aspect. It should be noted that these functions model the acoustic field at the virtual position starting from the sensing of the acoustic field in one point of the cabin. However, the noise at the virtual position can be radiated or reflected from all the cabin walls, thus violating the causality constraint for which the noise should propagate from the physical to the virtual microphones.

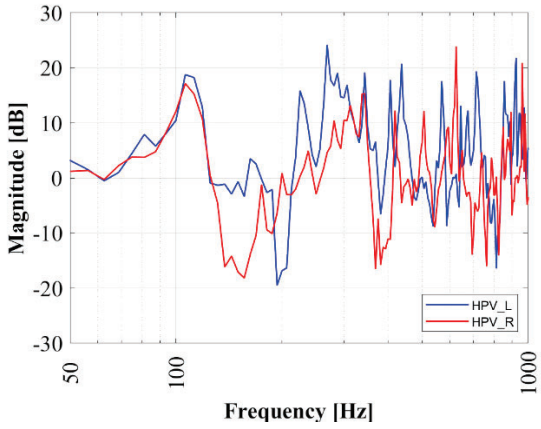

Fig. 6 – Funzioni di trasferimento fisico-virtuali lato sinistro (HPV_L) e lato destro (HPV_R)

Physical-virtual transfer functions of the left side (HPV_L) and the right side (HPV_R)

4.2 | Results for different signals

The results in terms of attenuation obtained in presence of a pure tone at 80 Hz, 100 Hz, 400 Hz and 700 Hz are shown in Fig. 7. The first two frequencies were chosen in the proximity of the cut-off frequency of the control loudspeakers, where the frequency response passes from a rising to a flat slope. The last one represents the maximum frequency considered for the development of the ANC system. The frequency of 400 Hz is a value chosen in the middle of this interval. The attenuation is defined as the difference between the initial noise level, with the ANC turned off, and the final noise level after the achievement of the convergence with the ANC system turned on. The attenuation reached on these frequencies should not be compared between each other, since the initial noise level depends on the position of microphones with respect to the cavity modes. For all the tested tones, the addition of the virtual sensing technique reduces the maximum attenuation reached with the same algorithm without the RMT, since the error signal is estimated and not directly measured at the target zone. The attenuation computed on the right side is lower than the one on the left side, with the exception of the algorithm with the RMT for the tone at 100 Hz, where the effect of the disturbance modelling are prevalent. The reason is that the initial noise level, without the ANC, is higher on the left side than the one on the right side. Thus, the system concentrates its effect on reducing the signal with the highest energy. The algorithm with the RMT is able to attenuate the noise on both sides for the tones at 100 Hz, 400 Hz and 700 Hz. For the tone at 80 Hz, it provides a small attenuation on the left side and a limited amplification on the right side. These results strongly depend on the modelling of the transfer functions HPL_L and HPV_R at each frequency and, thus, on the relative position between the physical and the virtual error microphones. It should be noted that the choice of another position for the physical microphones could provide better results, intercepting the signal coming from other directions.

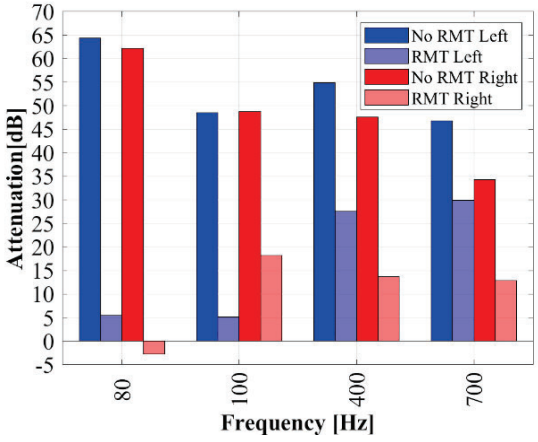

Fig. 7 – Attenuazione raggiunta con diversi toni puri
Attenuation reached with different pure tones

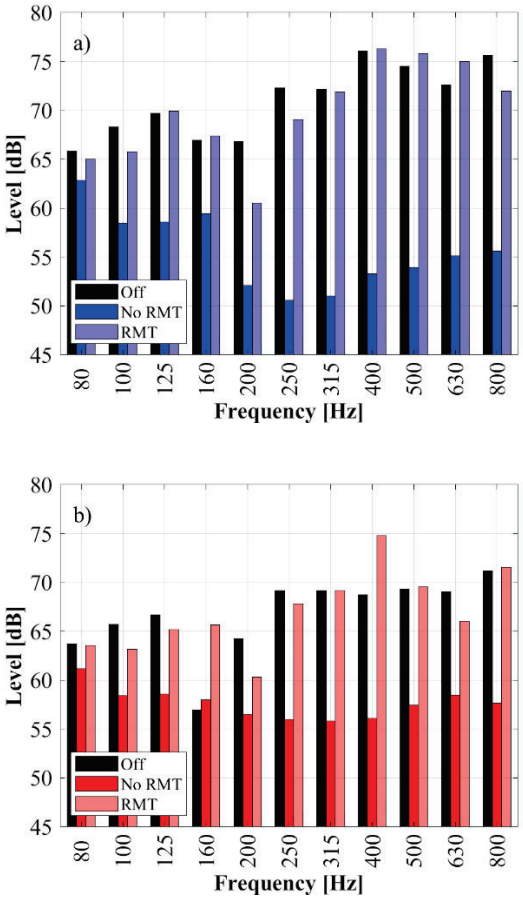

Fig. 8 – Livello di pressione sonora con un segnale di rumore pseudo-random: a) lato sinistro, b) lato destro
Sound pressure level with a pseudo-random noise signal: a) left side, b) right side

Secondly, a pseudo-random noise signal was used for the evaluation of the performance. This signal combines characteristics of both pure tones and white noise: like white noise, it contains a broad range of frequencies, but like pure tones, it maintains a periodic pattern, repeating every 0.1 s. Thus, it can be seen as an intermediate case between a pure tone and a pure broadband noise. The results in presence of this signal are illustrated in Fig. 8. In this case, the algorithm with a direct cancellation at the ears attenuates the noise in all the bands of interest, concentrating its effect on the bands between 200 Hz and 800 Hz. On the other hand, the algorithm with RMT shows more difficulties in providing a good noise cancellation. The RMT was able to attenuate the noise in some bands, for instance at 200 Hz and 250 Hz, even though without reaching the same good performance of the algorithm without the virtual technique. Furthermore, the RMT generated some amplifications in the bands of 160 Hz and 400 Hz on the right side, bringing the noise to a level similar to the left side.

Finally, the tests were carried out in presence of a pure white noise. This signal can be imagined as the previous pseudo-random noise signal, in which the periodicity is removed. The results are reported in Fig. 9. The performance of the algorithm with the RMT becomes comparable to that

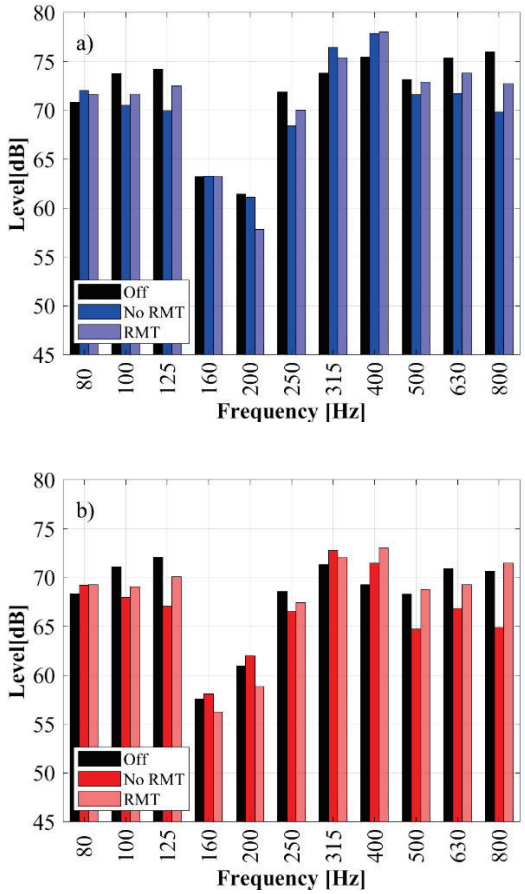

Fig. 9 – Livello di pressione sonora con un segnale di rumore bianco: a) lato sinistro, b) lato destro

Sound pressure level with a white noise signal: a) left side, b) right side

one of the basic algorithm without a virtual technique. The RMT attenuates the noise between the bands of 100 Hz and 250 Hz on both sides, overcoming the performance of the algorithm without a virtual technique in the band of 200 Hz. On the other hand, it generates an amplification similar to the one provided by the basic algorithm in the bands of 315 Hz and 400 Hz and attenuates the noise between 500 Hz and 800 Hz on the left side. The limited capability of attenuation in the presence of a broadband signal for both the algorithms can be related to the LMS procedure: since the updating of the adaptive filters occurs in an iterative way, the lack of periodicity does not allow the coefficients to converge quickly to an optimal value. Furthermore, the radiation and the reflection of noise from all the cabin walls increment the complexity of the problem, in particular for the algorithm with RMT, which is not able to model the noise which propagates without respecting the causality constraint between the physical and the virtual positions.

The results in terms of overall attenuation are reported in Tab. 1 and Tab. 2 for the pseudo-random noise and the white noise signals respectively. Comparing the two tables, it can be observed that the removal of the periodicity affects in particular the algorithm without the RMT. The ANC system with the RMT provides a small overall attenuation on the left side and an amplification on the right side. However, it should be noted that the initial overall noise level was 3 dB lower on the right side for both the pseudo-random and the white noise signals and, thus, this amplification is considered acceptable if it provides attenuation on the loudest side.

Tab. 1 –Attenuazione globale per rumore pseudo-random

Overall attenuation for a pseudo-random noise signal

	No RMT		*RMT*	
Side	Left	Right	Left	Right
Attenuation [dB]	15.1	10.0	0.3	–1.0
Attenuation [dB(A)]	19.5	12.1	0.3	–0.9

Tab. 2 – Attenuazione globale per rumore bianco

Overall attenuation for a white noise signal

	No RMT		*RMT*	
Side	Left	Right	Left	Right
Attenuation [dB]	0.9	1.4	0.3	–0.1
Attenuation [dB(A)]	1.8	2.2	0.8	–0.5

4.3 | Extension of the zone of quiet

In a free field condition, the extension of the zone of quiet where a mean reduction of 10 dB occurs is estimated as one tenth of the acoustic wavelength [37]. The shape of this region can change in a confined space such as in the presence of obstacles, due to the reflections and to diffraction effects. Furthermore, the shape depends on the number of actuators and sensors involved in the ANC system. In this case study, the extension of the part of the zone of quiet on the left side, the loudest one, is monitored through an array of three microphones, not involved in the ANC system and placed in line with a spacing of 5 cm. The results are shown in Fig. 10 for the tones with a frequency of 100 Hz and 400 Hz respectively. In absence of a virtual technique, the zone of quiet created by the ANC system is centred onto the error microphone, where the initial noise level is brought to the background noise level for all the tested tones. For the tone at 100 Hz (Fig. 10(a)), the attenuation obtained without the RMT is concentrated mainly on the first 5 cm. When the RMT is employed, the attenuation is more limited, but is maintained constant with the distance. A similar graph can be obtained with the tone at 80 Hz. In the presence of a tone with a frequency of 400 Hz (Fig. 10(b)), the attenuation is similar to the previous case in the first 10 cm for the algorithm without the RMT. However, the algorithm employing the RMT provides a larger attenuation with respect to the previous case, becoming comparable to the case without the RMT for a distance beyond 5 cm. For a tone at 700 Hz, not reported in these graphs, the attenuation is important strictly in the first 5 cm from the ear for both the algorithms, while it becomes limited for higher distances assuming similar values for the

two algorithms. Since the distance between the two ears was about 15 cm, this fact suggests that two small zones of quiet are created for this frequency, one in the proximity of each ear. In general terms, no amplification was sensed in the analysed acoustic field for all the employed tones. The increment of the disturbing tonal frequency reduces the extension of the zone of quiet. The shape depends on the tonal frequency combined with the modal effects inside the cabin.

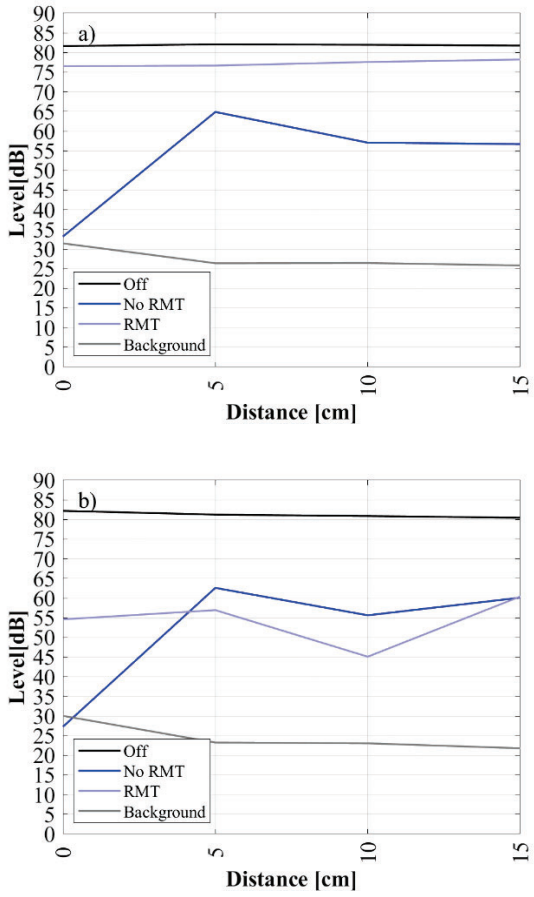

Fig. 10 – Estensione della zona di quiete per I toni a a) 100 Hz e b) 400 Hz

Extension of the zone of quiet for the tones at a) 100 Hz and b) 400 Hz

The same analysis was conducted with the pseudo-random noise signal. Since this type of noise excites a broad range of frequencies, the results were analysed as spectrograms as a function of the distance from the ear and of the frequency. The results are reported in Fig. 11 for the cases without and with the RMT respectively. Observing the case without the virtual sensing technique in Fig. 11(a), the zone of quiet extends beyond 15 cm for the frequency bands from 160 Hz to 500 Hz, with a higher performance at 250 Hz and 500 Hz. In the first 5 cm, all the bands are interested by a significant attenuation. The bands between 160 Hz and 200 Hz show a lower attenuation with respect to the range between 200 Hz and 500 Hz. However, it should be noted that the virtual error microphones fall into a nodal position for the cavity modes, making these contributions less relevant for the overall noise level. For high frequencies and for a distance larger than 10 cm, the ANC system provides an amplification larger than 1 dB. When the RMT is employed (Fig. 11(b)), the values of the attenuation are more limited and the zone of quiet extends up to 15 cm only for the bands between 160 Hz and 250 Hz. The area with an amplification larger than 1 dB is more extended with respect to the previous case. In particular, this amplification reaches the error microphone for the band of 630 Hz. This aspect is strongly related to the preliminary modelling stages, in particular to the one of the physical-virtual impulse response, which is not able to consider the noise coming from different directions inside the cabin. Furthermore, the influence of the cavity modes combined with the modelling error of the acoustic field in the algorithm, can provide different shapes of the zone of quiet, with the highest attenuation not centred on the target zone.

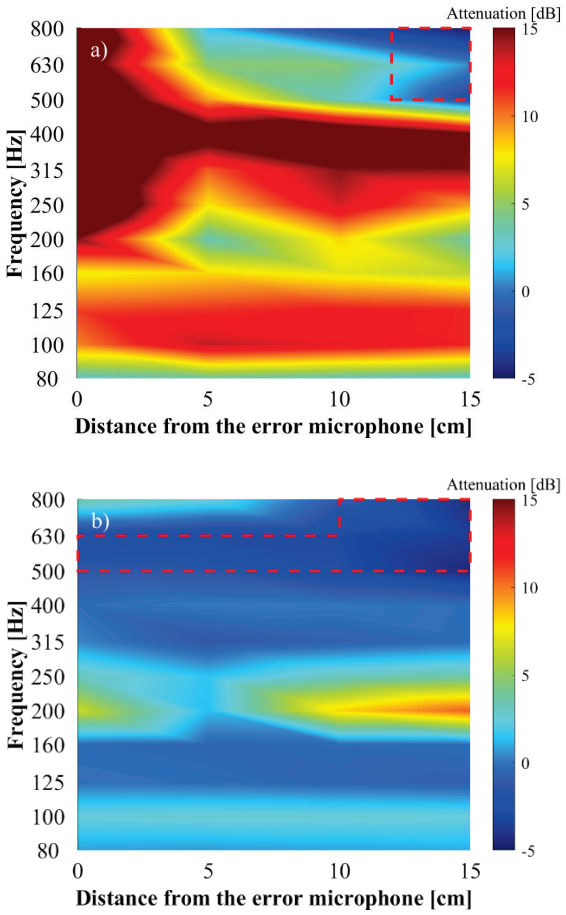

Fig. 11 – Estensione della zona di quiete per segnale di rumore pseudo-random: a) senza RMT, b) con RMT (la linea tratteggiata evidenzia l'area con amplificazione maggiore di 1 dB)

Extension of the zone of quiet for the pseudo-random noise signal: a) without the RMT, b) with the RMT (the dashed line highlights the area with amplification larger than 1 dB)

Finally, to demonstrate that the performance of the ANC system with the RMT is dependent on the type of environment, a comparison with the attenuation reached in a free field condition, assuming same distances between microphones and loudspeakers, is shown in Fig. 12 for the tones

at 100 Hz and 400 Hz. As it can be observed, in absence of reflections causing non-causal noise propagation, the attenuation reaches higher values, overcoming the performance obtained inside the enclosure.

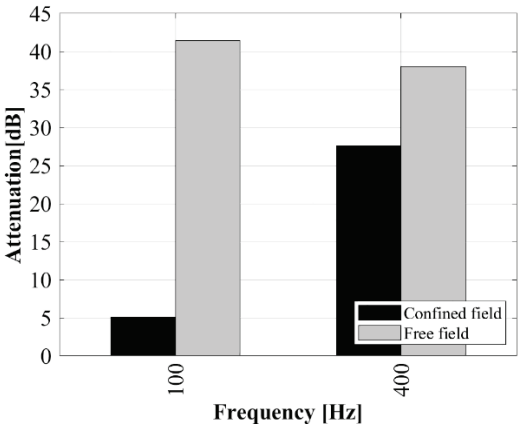

Fig. 12 – Confronto dell'attenuazione raggiunta con RMT per due toni puri in condizioni di campo libero e in campo confinato
Comparison of the attenuation reached with the RMT for two pure tones in a free field and confined field conditions

5 | Conclusions

In this paper, an evaluation of the effectiveness of an ANC system with the RMT applied to a tractor cabin was carried out. This system was analysed in a multi-channel configuration considering different typologies of disturbing signals. The results show that the ANC system produces a lower attenuation with respect to the algorithm with a direct cancellation of the noise at the ears. However, it should be noted that in a real-world application, the error microphones cannot be positioned near the target zone, but need to be placed far away. Moreover, the performance of the ANC system decreases with the complexity of the disturbing signal, passing from a periodic narrowband signal to a non-periodic broadband one. This happens both with and without the RMT. However, the internal modelling of the disturbance signals at the virtual positions provides a higher degradation of the performance, passing from a tonal noise to a pseudo-random noise. On the other hand, the results for a pure broadband noise are comparable for systems with and without the virtual sensing technique. Finally, the extension of the zone of quiet on the loudest side was monitored through an array of microphones. It emerged that the extension of this zone is dependent on the disturbing frequency and on the type of signal. Furthermore, the shape of the zone of quiet is strongly affected by the cavity modes, which could determine attenuation or amplification regions. In none of the cases with a tonal noise an amplification was sensed far from the target zone. However, for a pseudo-random noise signal, amplification of the noise can occur for high frequencies, in particular for a high distance from the ear. The general conclusions can be extended to any type of ANC system applied to an enclosure.

For a further development of this application, the number of physical error microphones could be incremented for a better estimation of the acoustic field at the virtual position. In particular, the placement of these microphones all around the cabin could prevent the violation of the causality constraint between the physical and the virtual positions, improving the modelling of the disturbance. However, the length of the filters and the usage of the resources of the control unit should be revised, due to a higher complexity of the system. After the improvement of this ANC system in lab, a validation of the performance on a real tractor should be carried out. In fact, the mechanism of excitation provided by the acoustic noise source, investing and putting in vibration primarily the frontal window of the cabin, can be different from the excitation provided by a real engine, making the whole structure radiating noise.

Conclusioni

In questo articolo è stata effettuata una valutazione dell'efficacia di un sistema ANC con RMT applicato alla cabina di un trattore. Questo sistema è stato analizzato in una configurazione multi-canale considerando diverse tipologie di segnali di disturbo. I risultati mostrano che il sistema ANC produce un'attenuazione inferiore rispetto all'algoritmo con una cancellazione diretta del rumore alle orecchie. Tuttavia, va notato che in un'applicazione reale i microfoni di errore non possono essere posizionati vicino alla zona target, ma devono essere collocati a una certa distanza. Inoltre, le prestazioni del sistema ANC diminuiscono con la complessità del segnale di disturbo, passando da un segnale periodico a banda stretta a uno non periodico a banda larga. Ciò avviene sia con sia senza RMT. Tuttavia, la modellazione interna dei segnali di disturbo nelle posizioni virtuali determina un maggior degrado delle prestazioni, passando da un rumore tonale a un rumore pseudo-random. D'altra parte, i risultati per un rumore puramente casuale sono comparabili per i sistemi con e senza la tecnica di rilevamento virtuale. Infine, l'estensione della zona di quiete sul lato più rumoroso è stata monitorata attraverso un array di microfoni. È emerso che l'estensione di questa zona dipende dalla frequenza del disturbo e dal tipo di segnale. Inoltre, la forma della zona di quiete è fortemente influenzata dai modi di cavità, che possono determinare regioni di attenuazione o amplificazione. In nessuno dei casi con rumore tonale è stata rilevata un'amplificazione lontano dalla zona target. Tuttavia, per un segnale di rumore pseudo-random, l'amplificazione del rumore può verificarsi per alte frequenze, in particolare a distanza dall'orecchio. Le conclusioni generali possono essere estese a qualsiasi tipo di sistema ANC applicato a un ambiente chiuso.

Per un ulteriore sviluppo di questa applicazione, il numero di microfoni di errore fisici potrebbe essere aumentato per una migliore stima del campo acustico nella posizione virtuale. In particolare, il posizionamento di questi microfoni attorno alla cabina potrebbe prevenire la violazione del vincolo di causalità tra le posizioni fisiche e virtuali, migliorando la modellazione del disturbo. Tuttavia, la lunghezza dei filtri e l'utilizzo delle risorse dell'unità di controllo dovrebbero essere rivisti a causa della maggiore complessità del sistema. A seguito del miglioramento di questo sistema ANC in laboratorio, dovrebbe essere effettuata una validazione delle prestazioni su un trattore reale. Infatti, il meccanismo di eccitazione fornito dalla

sorgente di rumore acustico, che investe e mette in vibrazione principalmente il vetro anteriore della cabina, potrebbe essere diverso dall'eccitazione fornita da un motore reale, che fa irradiare rumore all'intera struttura.

6 | Acknowledgement

This work was supported by the BRIC 2022 ID-11 project from INAIL (National Institute for Insurance against Accidents at Work).

References

[1] A. Pizzuti, A. Papale, L. A., P. Nataletti, I. Pinto, G. Campo, Sistema di sorveglianza delle malattie professionali: Ipoacusia da rumore un problema di salute ancora attuale sul lavoro, Inail, 2018.

[2] Relazione annuale 2021 del Presidente - Appendice statistica, Inail, 2022.

[3] G. Santoro, G. Vassalini, L. Ragni, G. Casini Ropa, La misura dell'esposizione al rumore in agricoltura, (1999).

[4] K.N. Dewangan, G.V.P. Kumar, V.K. Tewari, Noise characteristics of tractors and health effect on farmers, Appl. Acoust. 66 (2005) 1049–1062. https://doi.org/10.1016/j.apacoust.2005.01.002.

[5] J.D.C. Talamo, Effects of cab noise environment on the hearing perception of agricultural tractor drivers, Appl. Acoust. 12 (1979) 125–137. https://doi.org/10.1016/0003-682X(79)90030-6.

[6] V. Ravindran, B. Prakash, Agricultural tractor noise control, in: SAE 2013 Commer. Veh. Eng. Congr., 2013. https://doi.org/10.4271/2013-01-2342.

[7] S. Velioglu, A. Yıldız, M. Doganli, O. Tandogan, Interior noise analysis and prediction of a tractor cabin with emphasis on correlations with experimental data, in: SAE 2013 Noise Vib. Conf. Exhib., 2013. https://doi.org/10.4271/2013-01-1964.

[8] P.S. Yadav, A.A. Gaikwad, S.Y. Badgujar, Y.V. Surkutwar, N.V. Karanth, Noise reduction on agricultural tractor, in: Symp. Int. Automot. Technol. 2013, 2013. https://doi.org/10.4271/2013-26-0103.

[9] A.M. Abd-El-Tawwab, S.A. Abouel-Seoud, F.M. El-Sayed, T.A. Abd-El-Hakim, Characteristics of agriculture tractor interior noise, J. Low Freq. Noise Vib. Act. Control 19 (2000) 73–81. https://doi.org/10.1260/0263092001492822.

[10] J.P. Evans, R.T. Whyte, J.S. Price, J.M. Bacon, D.A. Semple, A.J. Scarlett, R.M. Stayner, Practical solutions to noise problems in agriculture, Health and Safety Executive, 2004.

[11] H.-W. Han, W.-H. Im, H.-J. Choi, S.-J. Cho, S.-D. Lee, Y.-J. Park, Effect of sound insulation on noise reduction in an agricultural tractor cab, Sci. Rep. 12 (2022) 22038. https://doi.org/10.1038/s41598-022-26408-3.

[12] D. Pessina, M. Guerretti, Effectiveness of hearing protection devices in the hazard reduction of noise from used tractors, J. Agric. Eng. Res. 75 (2000) 73–80. https://doi.org/10.1006/jaer.1999.0489.

[13] J. Jiang, Y. Li, Review of active noise control techniques with emphasis on sound quality enhancement, Appl. Acoust. 136 (2018) 139–148. https://doi.org/10.1016/j.apacoust.2018.02.021.

[14] S.J. Elliott, P.A. Nelson, Active noise control, IEEE Signal Process. Mag. 10 (1993) 12–35. https://doi.org/10.1109/79.248551.

[15] S.M. Kuo, D.R. Morgan, Active noise control: a tutorial review, Proc. IEEE 87 (1999) 943–975. https://doi.org/10.1109/5.763310.

[16] S.M. Kuo, I. Panahi, K.M. Chung, T. Horner, M. Nadeski, J. Chyan, Design of active noise control systems with the TMS320 family, (1996).

[17] Z. Zhang, C. Shi, X. Lv, Z. Ling, Active control of interior road noise using the remote microphone technique, INTER-NOISE NOISE-CON Congr. Conf. Proc. 265 (2023) 916–920. https://doi.org/10.3397/IN_2022_0130.

[18] W. Jung, S.J. Elliott, J. Cheer, Local active control of road noise inside a vehicle, Mech. Syst. Signal Process. 121 (2019) 144–157. https://doi.org/10.1016/j.ymssp.2018.11.003.

[19] S. Elliott, C.K. Lai, T. Vergez, J. Cheer, Robust stability and performance of local active control systems using virtual sensing, in: 23rd Int. Congr. Acoust., 2019.

[20] D. Moreau, B. Cazzolato, A. Zander, C. Petersen, A review of virtual sensing algorithms for active noise control, Algorithms 1 (2008) 69–99. https://doi.org/10.3390/a1020069.

[21] N. Jiang, C. Shi, H. Li, Y. Kajikawa, Near-field error sensing of multi-channel active noise control using virtual sensing technique, in: 25th Int. Congr. Sound Vib., 2018.

[22] P.S.S. Ahamed, P. Duraiswamy, Virtual sensing active noise control system with 2D microphone array for automotive applications, in: 2019 6th Int. Conf. Signal Process. Integr. Netw. SPIN, IEEE, Noida, India, 2019: pp. 151–155. https://doi.org/10.1109/SPIN.2019.8711608.

[23] R. Maeda, Y. Kajikawa, Comparisons of two virtual sensing methods for broadband noise, in: 23rd Int. Congr. Acoust., 2019.

[24] S. Turpati, V. Moram, Implementation of robust virtual sensing algorithm in active noise control to improve silence zone, Int. J. Speech Technol. 26 (2023) 51–62. https://doi.org/10.1007/s10772-021-09845-9.

[25] E. Sasaki, M. Kamata, A. Sano, Virtual error approach to direct multi-channel adaptive active noise control, in: 13th Int. Congr. Sound Vib., 2006.

[26] M. Pawelczyk, Polynomial approach to design of feedback virtual-microphone active noise control system, in: 13th Int. Congr. Sound Vib., 2006.

[27] I.T. Ardekani, W.H. Abdulla, An adaptive signal processing system for active control of sound in remote locations, in: 2013 Asia-Pac. Signal Inf. Process. Assoc. Annu. Summit Conf., IEEE, Kaohsiung, Taiwan, 2013: pp. 1–7. https://doi.org/10.1109/APSIPA.2013.6694322.

[28] I.T. Ardekani, W.H. Abdullah, S.U. Rehman, Remote FxLMS algorithm for active control of sound in remote locations, in: Signal Inf. Process. Assoc. Annu. Summit Conf. APSIPA 2014 Asia-Pac., IEEE, Chiang Mai, Thailand, 2014: pp. 1–5. https://doi.org/10.1109/APSIPA.2014.7041553.

[29] D.J. Moreau, B.S. Cazzolato, A.C. Zander, Active noise control at a moving virtual microphone using the SOTDF moving virtual sensing method, in: Proc. Acoust. 2009, 2009.

[30] S. Höber, C. Pape, E. Reithmeier, Generating a position-adaptive quiet zone in enclosed spaces, in: Internoise 2017, 2017.

[31] Y. Kajikawa, Y. Kajikawa, A Study on Improving the Robustness of Virtual Sensing Methods in ANC Systems, INTER-NOISE NOISE-CON Congr. Conf. Proc. 265 (2023) 5451–5458. https://doi.org/10.3397/IN_2022_0801.

[32] C.K. Lai, B. Lam, D. Shi, W.-S. Gan, Real-time modelling of observation filter in the remote microphone technique for an active noise control application, in: ICASSP 2023 - 2023 IEEE Int. Conf. Acoust. Speech Signal Process. ICASSP, IEEE, Rhodes Island, Greece, 2023: pp. 1–5. https://doi.org/10.1109/ICASSP49357.2023.10095752.

[33] S.J. Elliott, J. Garcia-Bonito, Active cancellation of pressure and pressure gradient in a diffuse sound field, J. Sound Vib. 186 (1995) 696–704. https://doi.org/10.1006/jsvi.1995.0482.

[34] F. Mori, A. Santoni, P. Fausti, F. Pompoli, P. Bonfiglio, P. Nataletti, The effectiveness of least mean squared-based adaptive algorithms for active noise control system in a small confined space, Appl. Sci. 13 (2023) 11173. https://doi.org/10.3390/app132011173.

[35] S.J. Elliott, W. Jung, J. Cheer, Causality and robustness in the remote sensing of acoustic pressure, with application to local active sound control, in: ICASSP 2019 - 2019 IEEE Int. Conf. Acoust. Speech Signal Process. ICASSP, IEEE, Brighton, United Kingdom, 2019: pp. 8484–8488. https://doi.org/10.1109/ICASSP.2019.8682474.

[36] D. Shi, B. Lam, W. Gan, Analysis of multichannel virtual sensing active noise control to overcome spatial correlation and causality constraints, in: ICASSP 2019 - 2019 IEEE Int. Conf. Acoust. Speech Signal Process. ICASSP, IEEE, Brighton, United Kingdom, 2019: pp. 8499–8503. https://doi.org/10.1109/ICASSP.2019.8682344.

[37] A. David, S.J. Elliott, Numerical studies of actively generated quiet zones, Appl. Acoust. 41 (1994) 63–79. https://doi.org/10.1016/0003-682X(94)90085-X.